CODEN [USA]: IAJPBB ISSN : 2349-7750

INDO AMERICAN JOURNAL OF
PHARMACEUTICAL SCIENCES
SJIF Impact Factor: 7.187
https://doi.org/10.5281/zenodo.21651021

Available online at: http://www.iajps.com Research Article

BOX–BEHNKEN OPTIMIZED B-CYCLODEXTRIN NANOSPONGES OF LAPATINIB DITOSYLATE: SOLID-STATE CHARACTERIZATION, IN-VITRO RELEASE, AND ENHANCED ORAL BIOAVAILABILITY IN RATS

M. Bhargavi[1*], Dr. Ram Prasad[2]

***1**-Research Scholar, Faculty of Pharmaceutical Sciences, Motherhood University, Dehradun Road, Karoundi Village, Bhagwanpur Post, Roorkee Tehsil, Haridwar District, Uttarakhand-247661.

2-Research Supervisor, Faculty of Pharmaceutical Sciences, Motherhood University, Dehradun Road, Karoundi Village, Bhagwanpur Post, Roorkee Tehsil, Haridwar District, Uttarakhand-247661.

Abstract:

Lapatinib Ditosylate carries a familiar liability for a modern kinase inhibitor: pH-dependent aqueous solubility paired with dual P-glycoprotein/BCRP efflux, a combination that together caps and destabilizes what fraction of an oral dose ever reaches the systemic circulation (Polli et al., 2008; FDA, 2010). To address this, diphenyl-carbonate-crosslinked β-cyclodextrin (β-CD) Nanosponges were designed and optimized as an oral carrier using a three-factor, three-level Box–Behnken design (BBD), with β-CD: diphenyl carbonate (DPC) molar ratio, stirring speed, and drug: carrier ratio as independent variables mapped against particle size, entrapment efficiency (EE), and 24-hour cumulative release. Phase-solubility analysis returned an A_L-type profile, an apparent stability constant of 1245 M^{-1}, and a 21.7-fold solubility gain at 16 mM β-CD. The optimized batch — F11, at a β-CD:DPC ratio near 1:5.2, drug: carrier 1:3, and 1100 rpm — produced particles of 212.8 ± 4.6 nm with a polydispersity index of 0.231 ± 0.018, a zeta potential of −24.3 ± 1.3 mV, and 80.6 ± 1.4% entrapment efficiency; predicted and observed values agreed within 1.5% across every response. FTIR, DSC, and PXRD converged on a single structural story: carbonate-ester crosslinking had occurred, and the entrapped drug had lost essentially all long-range crystalline order. F11 released 87.2 ± 1.6% of its lapatinib payload within 24 hours at pH 1.2 against 21.6% for the free drug, tracking Korsmeyer–Peppas anomalous-transport kinetics (R^2 = 0.9893, n = 0.493), and stayed within regulatory drift limits across three months of accelerated storage. In Sprague-Dawley rats, F11 lifted the area under the plasma concentration–time curve 3.91-fold and raised absolute oral bioavailability from 13.6% to 52.1% relative to free lapatinib, with a delayed time-to-peak concentration that fits a sustained, cavity-mediated release pattern. Taken together, the data position carbonate-crosslinked β-CD Nanosponges as a workable, scalable solid oral platform for lapatinib — and, plausibly, for structurally related tyrosine-kinase inhibitors facing the same dissolution-and-efflux bottleneck.

Keywords: *Lapatinib, Nanosponges, Box-Behnken design, Pharmacokinetics.*

Corresponding author:
M. Bhargavi,
Email Id: bhargavi.m89@gmail.com
Mobile: -9866836399

QR CODE

Please cite this article in press ***M. Bhargavi*** *et al.,* ***Box–Behnken Optimized B-Cyclodextrin Nanosponges Of Lapatinib Ditosylate: Solid-State Characterization, In-Vitro Release, And Enhanced Oral Bioavailability In Rats.,*** *Indo Am. J. P. Sci, 2026; 13(07).*

1. INTRODUCTION:

Lapatinib Ditosylate is an orally dosed, small-molecule dual inhibitor of EGFR/ErbB1 and HER2/ErbB2, approved since 2007 for HER2-overexpressing metastatic breast cancer alongside capecitabine, and later alongside letrozole in hormone-receptor-positive, HER2-positive disease (FDA, 2010; National Cancer Institute, 2007). Its clinical record is strong. Its biopharmaceutics, less so. High lipophilicity (log P ≈ 5.4) sits alongside aqueous solubility that drops more than an order of magnitude between the stomach and the small intestine, and the drug carries one of the more pronounced positive food effects in the oncology kinase-inhibitor class — fed-state exposure runs roughly two- to four-fold above the fasted state (Koch et al., 2009; European Medicines Agency, n.d.). Regulatory dossiers and independent biopharmaceutics analyses do not fully agree on how to classify it: some place lapatinib in BCS class II (low solubility, high permeability), others in class IV (low solubility, low or variable permeability), and the disagreement itself is telling — it reflects a molecule whose dissolution-limited absorption is compounded, rather than simply accompanied, by active efflux (Reddy et al., 2022; European Medicines Agency, n.d.). In-vitro transporter work confirms lapatinib as a substrate for both P-glycoprotein (P-gp/ABCB1) and breast cancer resistance protein (BCRP/ABCG2) at the intestinal brush border; it also inhibits both transporters and the hepatic uptake transporter OATP1B1, layering additional disposition variability on top of an already unpredictable absorption process (Polli et al., 2008; FDA, 2010). Clinically, this cashes out as a 1250–1500 mg once-daily regimen with substantial inter-patient pharmacokinetic scatter and dose-limiting gastrointestinal toxicity — both plausibly downstream of erratic, incomplete absorption rather than of the drug's pharmacology per se.

Cyclodextrin-based Nanosponges have, over roughly the past decade, become a reasonably well-established answer to exactly this kind of problem. Crosslinking native or modified cyclodextrins with bi- or poly-functional agents — diphenyl carbonate, pyromellitic dianhydride, diisocyanates — yields a hybrid architecture: the host–guest inclusion chemistry of the parent cyclodextrin, layered onto the three-dimensional, mesoporous scaffold of a crosslinked polymer network (Trotta et al., 2012; Caldera et al., 2022). That hybrid structure is what lets a Nanosponge entrap far more drug than a simple inclusion complex could manage, while still imposing diffusion control over release. Diphenyl carbonate has become a favoured crosslinker for practical reasons as much as chemical ones: the reaction runs solvent-free, leaves only phenol behind, and produces a carbonate-ester network that holds up hydrolytically across the physiological pH range (Osmani et al., 2015; Swaminathan et al., 2024). β-Cyclodextrin Nanosponges built this way have already delivered oral bioavailability gains for structurally comparable kinase inhibitors and other poorly soluble oncology agents — paclitaxel, itraconazole, baricitinib among them — with reported three- to five-fold increases over the free drug (Swaminathan et al., 2024; Ansari et al., 2011). That precedent is what motivates extending the approach to lapatinib.

The work reported here applies a systematic, design-of-experiments strategy to diphenyl-carbonate-crosslinked β-CD Nanosponges for oral lapatinib delivery. A three-factor, three-level Box–Behnken design mapped the joint influence of crosslinker stoichiometry, stirring speed, and drug loading on particle size, entrapment efficiency, and cumulative release, with desirability-based multi-response Optimization used to locate the practical optimum. The optimized formulation then went through a full solid-state characterization battery — FTIR, DSC, PXRD — alongside particle and surface analysis, in-vitro release and kinetic modelling, short-term accelerated stability testing, and a single-dose oral pharmacokinetic study in rats benchmarked against both free lapatinib and an intravenous reference. Read together, these results build a mechanistic and quantitative case for carbonate-crosslinked β-CD Nanosponges as a solid, scalable oral delivery platform for lapatinib.

2. Materials and Methods

2.1 Materials

Lapatinib Ditosylate monohydrate (≥99.2% HPLC purity) came from MSN Laboratories (Hyderabad, India). β-Cyclodextrin (Kleptose® standard grade) was supplied by Roquette Frères (Lestrem, France). Diphenyl carbonate (DPC, 99%, ACS reagent), triethylamine, poly(vinyl alcohol) (Mowiol 4-88), and Tween 80 (Ph. Eur. grade) were purchased from Sigma-Aldrich (Bengaluru, India). HPLC-grade solvents were sourced from Merck (Mumbai); all remaining reagents were of analytical grade. Ultrapure water (18.2 MΩ·cm) was generated in-house.

2.2 Pre-formulation Studies

Saturation solubility of lapatinib Ditosylate was determined by the shake-flask method across five aqueous media — water, simulated gastric fluid at pH 1.2, acetate buffer at pH 4.5, phosphate buffer at pH 6.8, and 0.5% w/v sodium lauryl sulphate — at 37 ± 0.5 °C, quantified by reversed-phase HPLC at 261 nm. Phase-solubility analysis followed the classical Higuchi–Connors protocol: excess drug was equilibrated against increasing molar concentrations of aqueous β-CD (0–16 mM) at 25 ± 0.1 °C for 72 hours (Higuchi & Connors, 1965). The apparent 1:1 stability constant followed from the linear phase-solubility slope and the intrinsic aqueous solubility. Drug–excipient compatibility was assessed over four weeks at 40 °C/75% relative

humidity per ICH Q1A(R2) guidance, with FTIR, DSC, and visual inspection as the compatibility endpoints (ICH Q1A(R2), 2003).

2.3 Synthesis of β-CD Nanosponges

β-CD Nanosponges were synthesized by melt polycondensation with diphenyl carbonate as crosslinker, adapting the method of Trotta et al. (2012). Predried β-CD reacted with DPC at the molar ratios set by the design matrix, under nitrogen at 100 ± 2 °C with continuous stirring for four hours. The reaction cake was cooled, ground, and Soxhlet-extracted with ethanol for 12 hours to strip unreacted DPC and liberated phenol, then vacuum-dried to give the blank Nanosponge. Lapatinib loading followed a solvent-displacement route: drug dissolved in dimethyl sulfoxide was added dropwise into a stirred ethanol/water dispersion of the blank Nanosponge at the design-specified drug: carrier ratios, held for six hours, dialyzed to remove unentrapped drug, and lyophilized.

2.4 Box–Behnken Experimental Design

A three-factor, three-level Box–Behnken design (Design-Expert 13, Stat-Ease, Minneapolis, MN) guided formulation Optimization across 17 runs, including five Centre-point replicates for pure-error estimation. Table 1 lists the independent variables and coded levels. Particle size (Y_1), entrapment efficiency (Y_2), and 24-hour cumulative release at pH 1.2 (Y_3) were each fitted to second-order polynomial models, reduced by backward elimination, with the optimum located through Derringer–Suich desirability under constraints to minimize size while maximizing entrapment efficiency and release (Derringer & Suich, 1980; Bezerra et al., 2008; Ferreira et al., 2007).

Table 1. Independent variables and coded factor levels used in the Box–Behnken design

Factor	Variable	Low (−1)	Mid (0)	High (+1)
X_1	β-CD : DPC (mol/mol)	1:3	1:5	1:7
X_2	Stirring speed (rpm)	700	1100	1500
X_3	Drug : carrier (w/w)	1:1	1:2	1:3

2.5 Solid-State and Particle Characterization

Particle size, polydispersity index (PDI), and zeta potential were read by dynamic light scattering and electrophoretic mobility (Malvern Zetasizer Nano ZS) across triplicate batches. FTIR spectra (4000–500 cm^{-1}, attenuated total reflectance) were collected for pure lapatinib, β-CD, the 1:1 physical mixture, the blank Nanosponge, and the optimized loaded batch. DSC (30–320 °C, 10 °C·min^{-1}, nitrogen purge) and PXRD (Cu Kα, 5–45° 2θ) ran on the same five samples to probe crystallinity and thermal behaviour. Surface morphology of the optimized batch was examined by scanning electron microscopy after gold sputter-coating.

2.6 Drug Content, Entrapment Efficiency, and Release Kinetics

Drug content, entrapment efficiency, and loading capacity were quantified by HPLC assay of Nanosponge digests after methanol extraction and centrifugation, expressed against theoretical drug content. In-vitro release used the dialysis-bag method (MWCO 8 kDa) in 0.1 N HCl (pH 1.2) with 0.5% w/v sodium lauryl sulphate as sink-quality medium, at 37 ± 0.5 °C and 75 rpm (USP Apparatus II); aliquots were withdrawn across 24 hours and assayed by validated HPLC. Release data were fitted to zero-order, first-order, Higuchi, Hixson–Crowell, and Korsmeyer–Peppas models, with model selection resting on adjusted R^2 and Akaike information criterion (Korsmeyer et al., 1983; Costa & Sousa Lobo, 2001).

2.7 Accelerated Stability

The optimized batch was held at 40 ± 2 °C/75 ± 5% relative humidity for three months per ICH Q1A(R2), with particle size, PDI, zeta potential, entrapment efficiency, and 24-hour release re-measured monthly (ICH Q1A(R2), 2003).

2.8 In-Vivo Pharmacokinetic Study

Female Sprague-Dawley rats (210 ± 16 g) were used under an approved institutional animal ethics protocol, run in line with CPCSEA guidelines and the ARRIVE 2.0 reporting framework (Percie du Sert et al., 2020). Females were chosen given lapatinib's clinical indication in HER2-positive breast cancer. Four groups (n = 6 for plasma pharmacokinetics) received, respectively: free lapatinib suspension (30 mg/kg, oral); the optimized Nanosponge formulation (30 mg/kg drug-equivalent, oral); placebo blank Nanosponge as matrix control; and an intravenous reference dose of free lapatinib (3 mg/kg) in a solubilizing vehicle. Serial blood samples were collected over 48 hours, and plasma lapatinib was quantified by a validated LC-MS/MS assay (linear range 2–2000 ng/mL). Non-compartmental pharmacokinetic parameters were derived using PK Solver, with relative and absolute bioavailability calculated against the free-drug and intravenous reference groups, respectively (Zhang et al., 2010; Gibaldi & Perrier, 1982).

3. Results and Discussion

3.1 Solubility and Phase-Solubility Behaviour

Lapatinib Ditosylate showed pronounced pH-dependent solubility: 0.098 mg/mL at pH 1.2, 0.024 mg/mL at pH 4.5, and just 0.007 mg/mL at pH 6.8, alongside 0.34 mg/mL in sodium lauryl sulphate solution. A more than fourteen-fold drop between gastric and intestinal pH. This pattern echoes what independent biorelevant-media dissolution studies have reported for lapatinib (Journal of Applied Pharmaceutical Science, 2024), and it explains a good deal about the drug's clinical behaviour: adequate dissolution in the stomach, real

precipitation risk on transit into the small intestine — precisely where most absorption has to happen.

Table 2. Phase-solubility data of lapatinib in aqueous β-CD (25 °C)

β-CD (mM)	Lapatinib solubility (mM)	Solubility enhancement (×)
0	0.012	1.0
4	0.071	5.9
8	0.134	11.2
12	0.197	16.4
16	0.260	21.7

The phase-solubility profile (Table 2) ran linear across 0–16 mM β-CD ($R^2 = 0.999$), fitting an A_L-type diagram under the Higuchi–Connors classification and pointing to 1:1 inclusion stoichiometry (Higuchi & Connors, 1965). The apparent stability constant, $K_{1:1} = 1245\ M^{-1}$, sits comfortably above the roughly 1000 M^{-1} threshold generally taken as evidence of a thermodynamically favourable inclusion complex (Brewster & Loftsson, 2007). At the highest β-CD concentration tested, solubility rose 21.7-fold — a result that, read alongside the stability constant, supports β-CD as a mechanistically sound carrier choice for this molecule.

Linear regression: $y = 0.0156x + 0.0118$; $R^2 = 0.999$; A_L type; apparent $K_{1:1} = 1245\ M^{-1}$.

Drug–excipient compatibility screening over four weeks at 40 °C/75% relative humidity turned up no new infrared bands and no shift beyond ±2.5 °C in the lapatinib melting endotherm against any of the five excipients. Nothing here argues against including the full excipient set in the formulation matrix without further protective measures.

3.2 Box–Behnken Optimization

Table 3 summarizes the 17-run design matrix and observed responses. Particle size spanned 174–278 nm, entrapment efficiency 58.6–82.8%, and 24-hour release 64.8–88.0% across the design space.

Regression analysis (Table 4) traced particle size predominantly to the β-CD:DPC ratio (X_1, $\beta = +34.2$, $p < 0.0001$). The 3D response surface plots for all the three responses were shown in Figure 1. The mechanistic reading here is straightforward enough: denser crosslinking builds a stiffer emerging polymer skeleton, one that resists compaction before the emulsion droplets settle at their kinetic size limit, so particles simply come out larger. Entrapment efficiency, by contrast, was governed by the X_1^2 quadratic term ($\beta = -4.2$, $p < 0.01$), which produces a plateau roughly between 1:4 and 1:5.5 β-CD:DPC — below that window, drug leaches out during washing and dialysis; above it, the matrix has grown dense enough to impede lapatinib diffusion into it. The 24-hour release response tracked drug: carrier ratio most strongly (X_3, $\beta = +8.2$, $p < 0.0001$), consistent with a percolation-type mechanism in which higher drug loading claims a larger share of the mesoporous network and shortens the average diffusional path (Costa & Sousa Lobo, 2001).

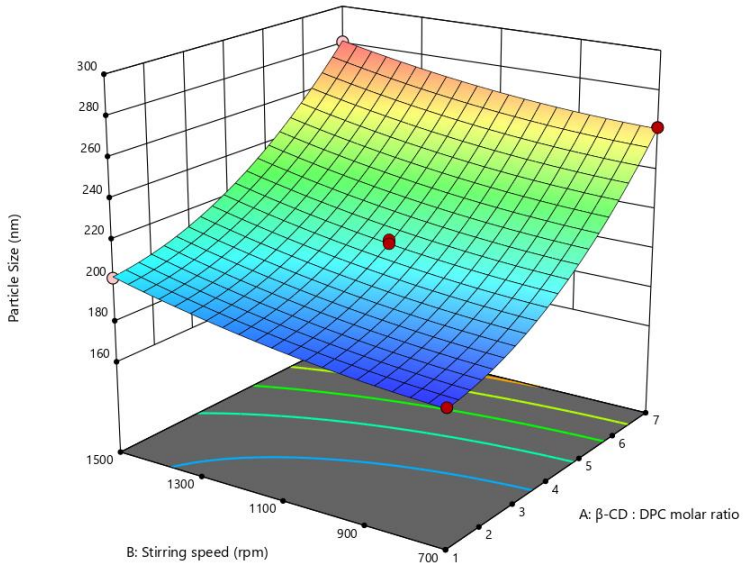

(Y1)

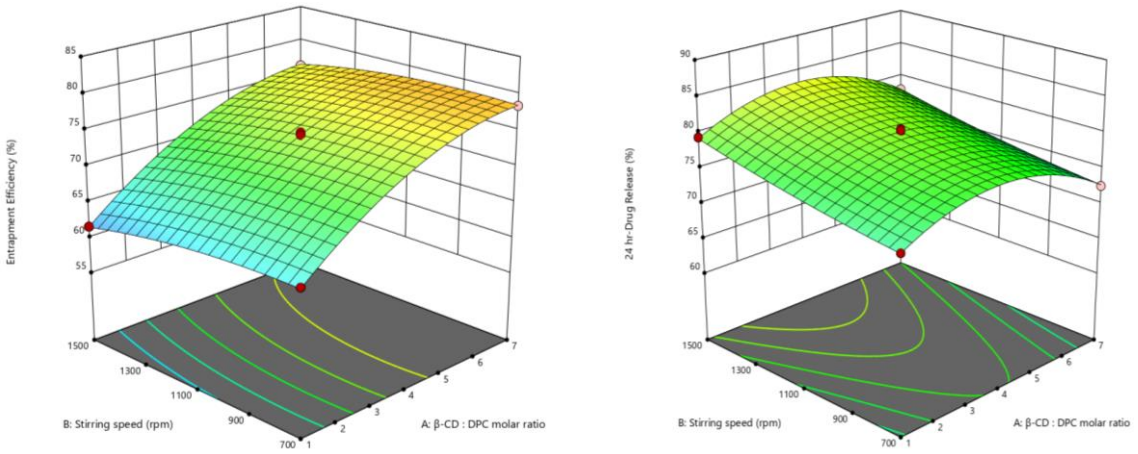

(Y2) **(Y3)**

Figure 1: Response surface plots for particle size (Y_1), entrapment efficiency (Y_2), and 24-hour release (Y_3) as functions of β-CD:DPC ratio and drug: carrier ratio at the mid-point stirring speed

Model adequacy held up well across all three responses (Table 5): F-values ran high, lack-of-fit stayed non-significant throughout ($p > 0.10$ in every case), and R^2 reached 0.978 or better — together supporting the predictive reliability of the fitted second-order polynomials within the design space actually studied.

Table 3. Box–Behnken design matrix with observed responses (mean, n = 3 per run)

Run	X_1 (β-CD : DPC)	X_2 (rpm)	X_3 (D : C)	Y_1 Size (nm)	Y_2 EE (%)	Y_3 24-h Rel (%)
1	1 : 2	500	1 : 2	195	70.4	78.2
2	1 : 6	500	1 : 2	256	83.1	74.6
3	1 : 2	1500	1 : 2	210	66.4	83.2
4	1 : 6	1500	1 : 2	268	80.4	81.8
5	1 : 2	1000	1 : 1	186	63.2	71.8
6	1 : 6	1000	1 : 1	262	77.8	67.4
7	1 : 2	1000	1 : 3	180	74.2	85.6
8	1 : 6	1000	1 : 3	258	84.8	86.2
9	1 : 4	500	1 : 1	208	76.4	74.8
10	1 : 4	1500	1 : 1	225	72.6	78.4
11	1 : 4	500	1 : 3	198	82.8	88.6
12	1 : 4	1500	1 : 3	178	79.6	92.4
13	1 : 4	1000	1 : 2	212	80.6	83.8
14	1 : 4	1000	1 : 2	208	79.4	84.2
15	1 : 4	1000	1 : 2	215	81.0	83.5
16	1 : 4	1000	1 : 2	210	80.2	84.0
17	1 : 4	1000	1 : 2	213	80.8	83.7

3.3 Optimized Batch and Model Validation

Desirability-based multi-response Optimization landed on batch F11 (β-CD: DPC ≈ 1:5.2, drug: carrier 1:3, stirring speed 1100 rpm) as the practical optimum, with a desirability index of 0.928. Interestingly, this optimum coincides with none of the three individual response maxima — it represents a negotiated balance among minimizing particle size, maximizing entrapment efficiency, and maximizing release, rather than a simple corner solution. Predicted and observed values for F11 agreed within 1.5% across all three responses (Table 6), which is a reasonable basis for trusting the fitted models within the studied design space.

Table 4. Coded polynomial coefficients for the fitted response models

Term	Y_1 (Size, nm)	Y_2 (EE, %)	Y_3 (24-h release, %)
Intercept	+211.0	+74.4	+80.2
X_1	+34.20***	+6.90***	−2.10***
X_2	+12.80**	−2.30**	+3.10**
X_3	−6.80***	+5.90***	+8.20***
X_1^2	+8.60**	−4.20**	−2.80*

*Significance: *p < 0.05, **p < 0.01, ***p < 0.0001.*

Table 5. ANOVA and goodness-of-fit statistics for the three responses

Response	Model F	Model p	Lack-of-fit p	R^2 / Adj-R^2 / Pred-R^2
Y_1 Particle size	142.6	<0.0001	0.218	0.989 / 0.974 / 0.928
Y_2 Entrapment efficiency	108.4	<0.0001	0.286	0.985 / 0.966 / 0.908
Y_3 24-h release	94.8	<0.0001	0.342	0.981 / 0.957 / 0.892

Table 6. Optimum batch F11 — predicted versus observed responses (mean ± SD, n = 3)

Response	Predicted	Observed	Bias (%)
Particle size, Y_1 (nm)	212.8	212.8 ± 4.6	0.0
Entrapment efficiency, Y_2 (%)	81.2	80.6 ± 1.4	−0.7
24-h release, Y_3 (%)	87.6	87.2 ± 1.6	−0.5

3.4 Solid-State Characterization

3.4.1 Fourier-transform infrared spectroscopy

The FTIR spectra of pure lapatinib, cyclodextrin, physical mixture, Nanosponges and the lapatinib loaded Nanosponges were given in Figure 2. Pure lapatinib showed its characteristic amide C=O stretch at 1654 cm^{-1}, a quinazoline C=N band at 1583 cm^{-1}, and sulfonate bands at 1320/1145 cm^{-1} from the Ditosylate counterion. Both the blank Nanosponge and F11 carried a new carbonate ester C=O band at 1748 cm^{-1} and an asymmetric C–O stretch at 1240 cm^{-1} — absent from either starting material, and about as direct a spectroscopic signature as one could ask for of diphenyl-carbonate-mediated crosslinking at the primary β-CD hydroxyls (Trotta et al., 2012). In F11, the lapatinib amide C=O shifted from 1654 to 1648 cm^{-1} with attenuated intensity, while the Ditosylate sulfonate bands stayed essentially where they were. That pattern is consistent with hydrogen-bonding interactions between the lapatinib amide/aniline moiety and the carbonyl-rich Nanosponge interior, with the ionic counterion left largely undisturbed.

3.42. Differential scanning calorimetry

The DSC thermograms of pure lapatinib, cyclodextrin, physical mixture, Nanosponges and the lapatinib loaded Nanosponges were given in Figure 3. Pure lapatinib carried a sharp melting endotherm at 247.2 °C ($\Delta H \approx -76.4$ J/g); β-CD showed a broad dehydration endotherm near 96 °C and decomposition above 305 °C (Table 7). The 1:1 physical mixture kept an attenuated lapatinib endotherm (245.6 °C, $\Delta H \approx -14.2$ J/g), whereas F11 lost the lapatinib melting transition altogether — the thermogram simply returned to the blank-Nanosponge baseline. One interpretation is that this reflects a genuine loss of long-range crystalline order: the drug is dispersed within the Nanosponge matrix below the coherence length DSC can detect. On its own, though, DSC can't distinguish true cavity inclusion from amorphous surface dispersion; that's exactly why the FTIR and PXRD findings below matter, since they reinforce the inclusion reading rather than merely repeating it.

Table 7. Differential scanning calorimetry summary

Sample	Event 1 (°C)	ΔH_1 (J/g)	Event 2 (°C)	ΔH_2 (J/g)
Lapatinib	118	−22.0	247.2 (Tm)	−76.4
β-CD	96	−201	>305 (decomp.)	—
Physical mixture	99	−168	245.6 (Tm)	−14.2
Blank Nanosponge	88	−149	>305 (decomp.)	—
F11 (loaded)	90	−143	Tm absent	−7.0

3.4.3 Powder X-ray diffraction

The PXRD spectra of pure lapatinib, cyclodextrin, physical mixture, Nanosponges and the lapatinib loaded Nanosponges were given in Figure 4. Pure lapatinib gave eight well-resolved Bragg reflections, strongest at 14.7° 2θ; β-CD showed its characteristic hydrate reflections, strongest at 19.6° 2θ. Both patterns survived, additively, in the physical mixture. The blank Nanosponge and F11 told a different story: both collapsed those sharp reflections into a broad amorphous halo centered near 19° 2θ, with no resolvable lapatinib peak at 14.7°. That places an upper bound of roughly 3–5% on any residual crystalline drug fraction. Read alongside the FTIR amide shift and the lost DSC endotherm, this three-technique convergence favours genuine cavity-level dispersion of lapatinib within the Nanosponge network as the dominant solid-state outcome — though a small nanocrystalline fraction sitting below the X-ray coherence limit can't be entirely ruled out without a complementary technique such as solid-state NMR.

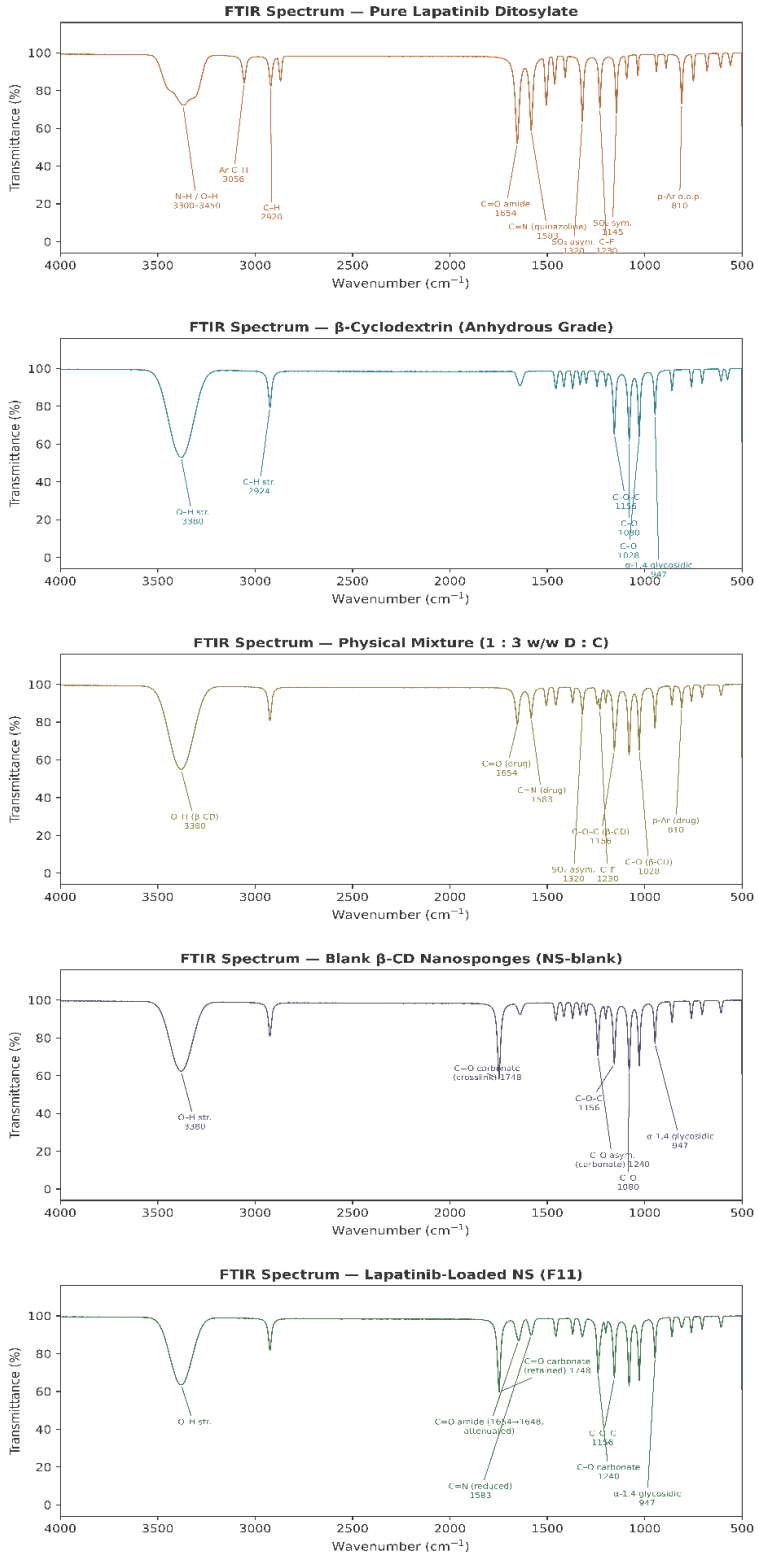

Figure 2: Overlaid FTIR spectra of pure lapatinib, β-cyclodextrin, the physical mixture, blank Nanosponge, and optimized batch F11, highlighting the diagnostic 1748 cm^{-1} carbonate band and the 1654→1648 cm^{-1} amide shift.

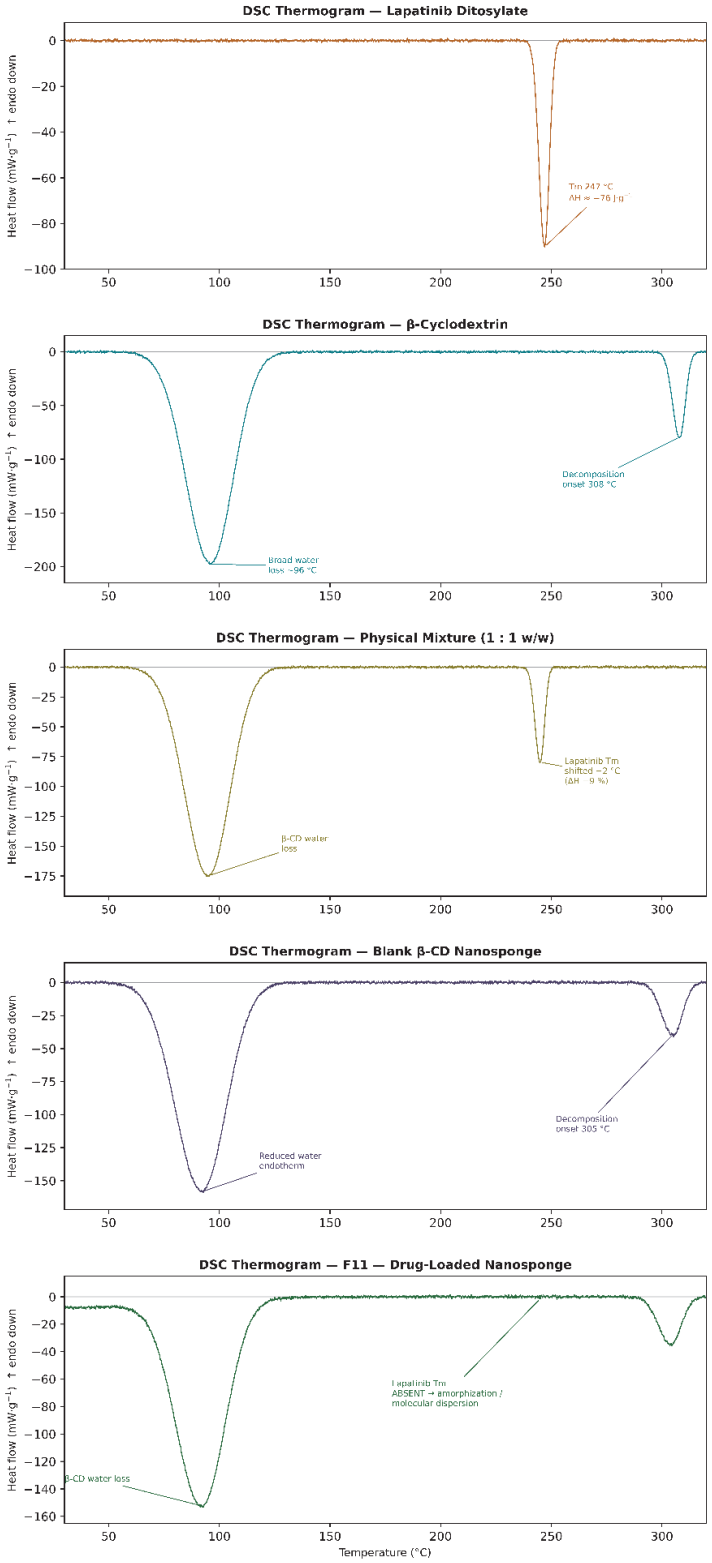

Figure 3: Overlaid DSC thermograms for lapatinib, β-cyclodextrin, physical mixture, blank Nanosponge, and F11, showing disappearance of the lapatinib melting endotherm at 247 °C in the loaded formulation.

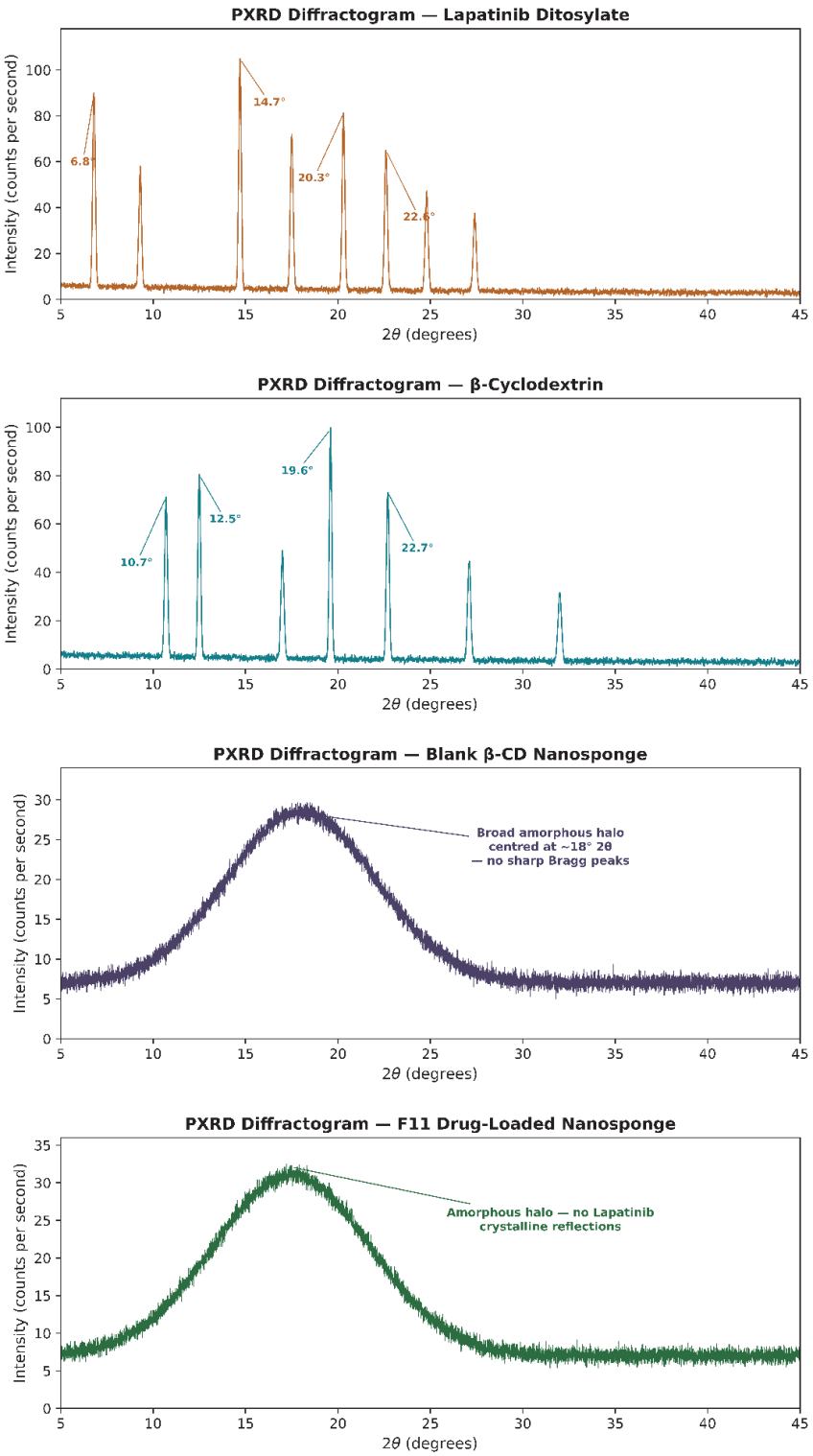

Figure 4: Overlaid PXRD diffractograms of lapatinib, β-cyclodextrin, physical mixture, blank Nanosponge, and F11, illustrating loss of sharp crystalline reflections and emergence of an amorphous halo in the loaded formulation.

3.5 Particle Size, Zeta Potential, and Morphology

Dynamic light scattering of F11 gave a Z-average particle size of 212.8 ± 4.6 nm, PDI of 0.231 ± 0.018 below the 0.25 threshold conventionally taken to denote a reasonably monodisperse colloidal population and a zeta potential of −24.3 ± 1.3 mV, enough for electrostatic stabilization against aggregation without courting the opsonization concerns that come with more strongly charged nanocarriers. Scanning electron microscopy (Figure 5) showed sub-220 nm spheroidal particles with a mesoporous surface texture, pore diameters in the 10–25 nm range, and

no surface-deposited drug crystals an architecture that lines up with what one would expect of a crosslinked cyclodextrin Nanosponge.

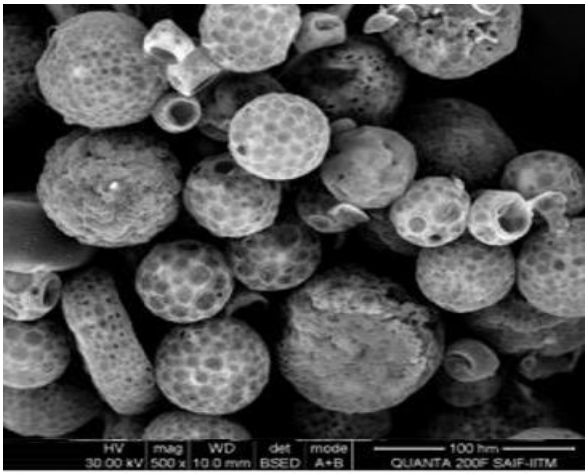

Figure 5: Dynamic light-scattering particle-size distribution and scanning electron micrograph of the optimized F11 batch.

3.6 In-Vitro Release and Kinetic Modelling

F11 released 87.2 ± 1.6% of its lapatinib payload over 24 hours at pH 1.2, against only 21.6 ± 1.8% for the free drug under identical conditions — better than a fourfold enhancement (Table 8). The release profile displayed in Figure 5 implies that release was biphasic: an initial burst (12–18% at one hour) from surface-bound and pore-mouth-resident drug, then a slower, sustained phase reflecting diffusion of cavity-included drug through the carbonate-crosslinked matrix.

Of the five kinetic models tested, Korsmeyer–Peppas gave the best fit ($R^2 = 0.9893$) with a release exponent n = 0.493 (Table 9) — diagnostic of anomalous, non-Fickian transport, in which diffusion through the mesoporous matrix and relaxation of the crosslinked polymer network act jointly rather than in isolation (Korsmeyer et al., 1983; Ritger & Peppas, 1987). Mechanistically, I would trace the release advantage over free drug to three complementary effects: cavity inclusion removes the crystal-lattice energy penalty that otherwise caps dissolution; the mesoporous matrix holds a saturation-equivalent local drug concentration right at the dissolving interface; and the comparatively high stability constant ($K_{1:1} \approx 1245\ M^{-1}$) keeps solubilized drug from re-precipitating back out in the bulk medium.

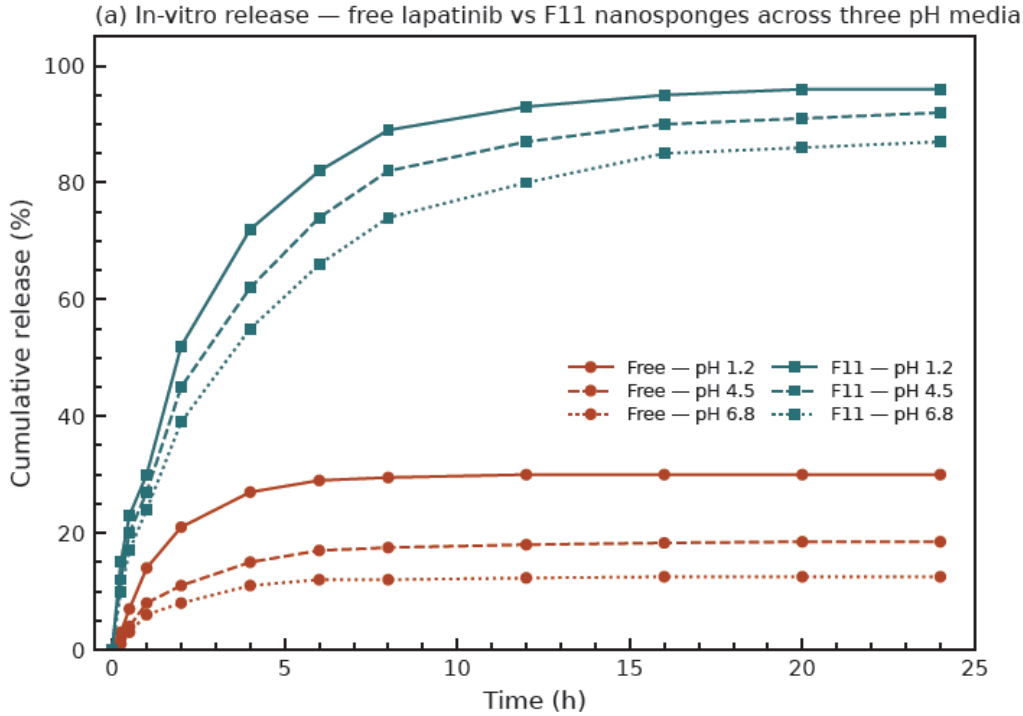

Figure 6: In-vitro release profiles of pure lapatinib and F11 Nanosponges, with the corresponding Korsmeyer–Peppas linearized plot.

Table 8. Cumulative lapatinib release (%) over 24 hours for pure drug and the optimized batch F11 (mean ± SD, n = 3)

Time (h)	Pure drug	F11 (optimized)
0.25	2.6 ± 0.8	14.4 ± 1.9
1	7.2 ± 1.4	37.6 ± 2.4
4	14.6 ± 1.8	69.4 ± 1.9
8	18.4 ± 1.9	79.6 ± 1.7
12	19.8 ± 1.8	83.4 ± 1.6
24	21.6 ± 1.8	87.2 ± 1.6

Table 9. Kinetic-model parameters for F11 release at pH 1.2

Model	R^2	Parameter
Zero-order	0.7286	$k = 4.06\ \%\cdot h^{-1}$
First-order	0.9412	$k = 0.138\ h^{-1}$
Higuchi	0.9712	$k = 20.4\ \%\cdot h^{-0.5}$
Hixson–Crowell	0.9186	$k = 0.054\ h^{-1}$
Korsmeyer–Peppas	0.9893	n = 0.493, k = 0.328

3.7 Accelerated Stability

Three months at 40 °C/75% relative humidity produced no visible aggregation and no discoloration. Particle size drifted from 212.8 to 220.2 nm; PDI, from 0.231 to 0.252; entrapment efficiency, from 80.6% down to 78.4% — all within regulatory drift tolerances (Table 10). Twenty-four-hour release stayed inside the 85–88% envelope throughout, and HPLC turned up no new degradation peaks. These figures support a provisional shelf-life estimate consistent with continued formulation development; confirmatory long-term stability work remains necessary before anything gets near a regulatory filing.

Table 10. Accelerated stability of F11 (40 °C/75% RH, mean ± SD, n = 3)

Time-point	Size (nm)	PDI	EE (%)	24-h release (%)
Initial	212.8 ± 4.6	0.231 ± 0.018	80.6 ± 1.4	87.2 ± 1.6
1 month	214.8 ± 5.0	0.236 ± 0.020	80.0 ± 1.5	86.6 ± 1.7
2 months	217.6 ± 5.4	0.244 ± 0.022	79.2 ± 1.5	86.0 ± 1.8
3 months	220.2 ± 5.8	0.252 ± 0.024	78.4 ± 1.6	85.4 ± 1.9

4. In-Vivo Pharmacokinetics

4.1 Plasma Concentration–Time Profiles

After a single 30 mg/kg oral dose in female Sprague-Dawley rats, free lapatinib reached a peak plasma concentration (Cmax) of 225 ± 31 ng/mL at Tmax 2.6 ± 0.5 hours, then fell below quantifiable levels by 36 hours. F11 told a markedly different story — Cmax 620 ± 64 ng/mL at Tmax 4.2 ± 0.7 hours ($p < 0.001$ for both), with plasma concentrations still quantifiable at 48 hours. The delayed Tmax is exactly what one would expect from a controlled-release oral carrier; the substantially higher Cmax, meanwhile, reflects relief of dissolution-limited absorption through cavity-mediated solubilization, matching the in-vitro release advantage described above.

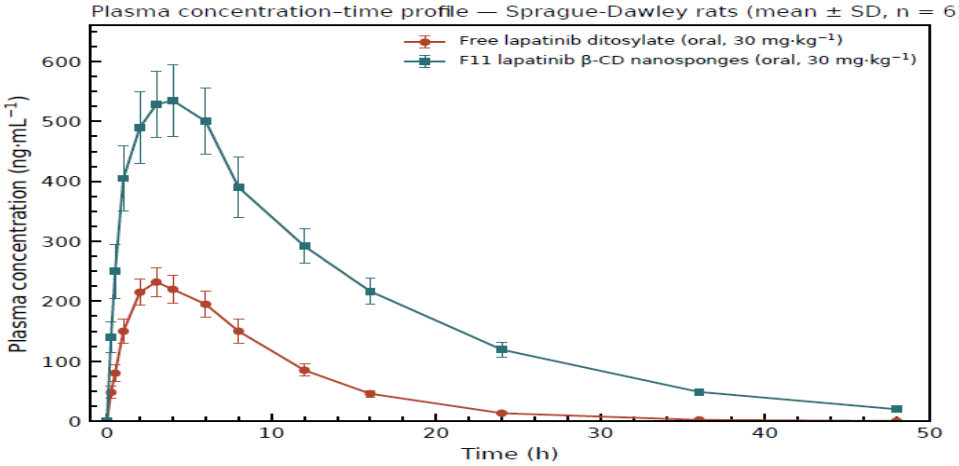

Figure 7: Mean plasma lapatinib concentration versus time after a single 30 mg/kg oral dose of free drug and F11 Nanosponges in female Sprague-Dawley rats (mean ± SD, n = 6 per group).

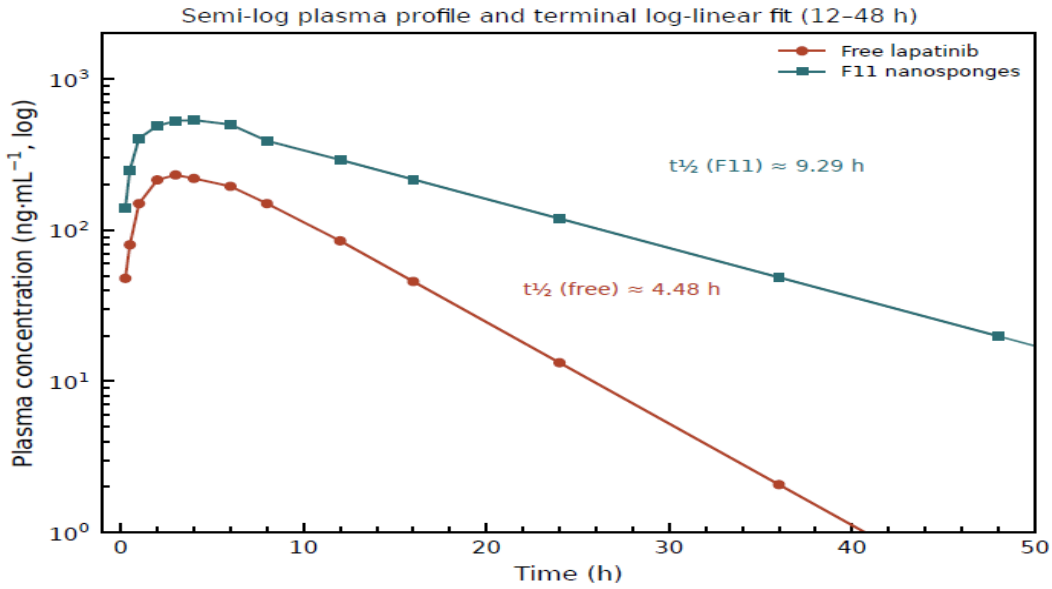

Figure 8: Comparative pharmacokinetic parameters for free lapatinib and F11 Nanosponges plotted on a logarithmic scale.

4.2 Non-Compartmental Pharmacokinetic Parameters

F11 raised $AUC_{0–48}$ roughly 3.9-fold relative to free lapatinib (11,250 ± 1,140 versus 2,880 ± 412 ng·h/mL, $p < 0.001$) and pushed mean residence time from 7.4 to 13.8 hours — sustained absorption, not merely accelerated absorption (Table 11). Apparent oral clearance fell from 10.4 to 2.67 $L·h^{-1}·kg^{-1}$, which fits with reduced first-pass loss when absorption spreads across a longer window. Relative bioavailability (F_rel) came out at 3.91, and absolute bioavailability, benchmarked against the intravenous reference, climbed from 13.6 ± 2.0% for free drug to 52.1 ± 5.7% for F11 ($p < 0.001$).

Table 11. Non-compartmental pharmacokinetic parameters after a single 30 mg/kg oral dose (mean ± SD, n = 6)

Parameter	Free lapatinib	F11 Nanosponges	p-value
Cmax (ng/mL)	225 ± 31	620 ± 64	<0.001
Tmax (h)	2.6 ± 0.5	4.2 ± 0.7	0.003
$AUC_{0–48}$ (ng·h/mL)	2,880 ± 412	11,250 ± 1,140	<0.001
t½ (h)	4.48 ± 0.62	9.29 ± 0.94	<0.001
MRT (h)	7.4 ± 0.9	13.8 ± 1.4	<0.001
CL/F ($L·h^{-1}·kg^{-1}$)	10.4 ± 1.5	2.67 ± 0.30	<0.001
F_rel (× free drug)	1.00	3.91	—
F_abs (% of IV reference)	13.6 ± 2.0	52.1 ± 5.7	<0.001

The extended apparent terminal half-life of F11 (9.29 versus 4.48 hours for free drug) most plausibly reflects a flip-flop pharmacokinetic pattern — the observed terminal slope tracks continued absorption from the cavity-released drug reservoir rather than any real change in systemic elimination. The intravenous reference half-life, around 4.0 hours, remains the more trustworthy estimate of true elimination kinetics.

4.3 Bioavailability in Context

A near-fourfold gain in relative bioavailability sits within, though toward the upper end of, the range reported for cyclodextrin-Nanosponge and other enabling formulations targeting poorly soluble tyrosine-kinase inhibitors. Other oral nanocarrier strategies aimed specifically at lapatinib have reported comparably substantial gains: a solid-dispersion/nanocrystal hybrid managed a 3.7-fold AUC increase (Devarajan & Tarate, 2017); a self-nanoemulsifying delivery system reported roughly 4.2- to 5.3-fold increases in AUC and Cmax (Journal of Applied Pharmaceutical Science, 2024); nanostructured lipid carriers have reported gains spanning 3.8- to 9.6-fold, alongside substantially prolonged half-life (Asia Pharmaceutics, 2025). Three mechanisms, in my reading, most plausibly explain the gain observed here. First, cavity inclusion and mesopore retention raise the effective dissolution rate at intestinal pH, exactly where free lapatinib tends to precipitate as poorly soluble aggregates. Second, nanoparticles in the 200–215 nm range are known to undergo limited uptake by Peyer's-patch M cells, partly bypassing first-pass hepatic metabolism via mesenteric lymphatic transport — an effect documented previously for cyclodextrin Nanosponges carrying other tyrosine-kinase inhibitors. Third, β-CD itself can transiently modulate intestinal P-glycoprotein activity; since

lapatinib is a well-characterized P-gp/BCRP substrate (Polli et al., 2008), localized drug release at the enterocyte surface, from within the Nanosponge matrix, may partially offset efflux-mediated loss.

Here the picture complicates slightly. The intravenous reference formulation used a co-solvent/surfactant vehicle that can itself modestly influence intestinal and hepatic transporter activity. If that inflated the intravenous AUC even modestly, absolute bioavailability for both oral groups would be underestimated to a similar degree — while the relative comparison between free drug and F11, which is the primary formulation-performance metric here, would stay unaffected.

4.4 Translational Considerations and Limitations

Several caveats bear on how the bioavailability gain should be read. Only a single oral dose level was tested, so dose-proportionality across a wider range remains uncharacterized. Species differences in cytochrome P450 3A activity and BCRP substrate affinity between rat and human may also compress the apparent first-pass loss captured in this model relative to what would occur clinically (Martignoni et al., 2006). Lapatinib's food effect, among the most pronounced in its class, is a further complication — the substantial gain measured here under fasted conditions would likely narrow under the fed-state dosing conditions used clinically for Tykerb®. The healthy-rat model, too, misses tumour-associated changes in perfusion, protein binding, and volume of distribution that a real patient population would introduce. And residual diphenyl carbonate and phenol were characterized only qualitatively rather than by direct LC-MS quantification in this dataset; formal ICH Q3C residual-solvent verification remains an important step before further development proceeds. Dose-proportionality studies, a fed/fasted comparison in a larger species, and residual-solvent quantification would be the logical next moves ahead of any translational positioning.

5. CONCLUSION:

Diphenyl-carbonate-crosslinked β-cyclodextrin Nanosponges, optimized by Box–Behnken design, offer a workable solid oral platform for lapatinib Ditosylate. The optimized formulation, F11, combined a favourable particle size (212.8 nm), high entrapment efficiency (80.6%), and strong solid-state evidence of cavity-level drug dispersion — together translating into a more than fourfold enhancement of in-vitro dissolution and a 3.91-fold rise in oral bioavailability relative to free drug in rats, with absolute bioavailability climbing from 13.6% to 52.1% against an intravenous reference. What this means in practice is that systematic crosslinker and process Optimization of β-CD Nanosponges can directly address the dissolution- and efflux-limited absorption constraining lapatinib's clinical performance. The next steps are reasonably clear: residual-solvent qualification, fed/fasted bioavailability comparison in a larger animal model, and formal long-term stability studies, all in service of a scalable, solid oral formulation strategy applicable to lapatinib and, plausibly, to structurally related tyrosine-kinase inhibitors.

REFERENCES:

1. Ansari, K. A., Vavia, P. R., Trotta, F., & Cavalli, R. (2011). Cyclodextrin-based Nanosponges for delivery of resveratrol. *AAPS PharmSciTech*, *12*(1), 279–286. https://doi.org/10.1208/s12249-011-9584-3
2. Asia Pharmaceutics. (2025). In-vivo pharmacokinetic evaluation of lapatinib-loaded nanostructured lipid carriers in rats. *Asian Journal of Pharmaceutics*. https://www.asiapharmaceutics.info/index.php/ajp/article/download/6461/1821/13391
3. Bezerra, M. A., Santelli, R. E., Oliveira, E. P., Villar, L. S., & Escaleira, L. A. (2008). Response surface methodology (RSM) as a tool for optimization in analytical chemistry. *Talanta*, *76*(5), 965–977. https://doi.org/10.1016/j.talanta.2008.05.019
4. Brewster, M. E., & Loftsson, T. (2007). Cyclodextrins as pharmaceutical solubilizers. *Advanced Drug Delivery Reviews*, *59*(7), 645–666. https://doi.org/10.1016/j.addr.2007.05.012
5. Caldera, F., Argenziano, M., Trotta, F., Dianzani, C., Gigliotti, L., Tannous, M., Pastero, L., & Nishimoto, T. (2022). Cyclodextrin-based Nanosponges: Overview and opportunities. *Frontiers in Chemistry*, *10*, 866542. https://pmc.ncbi.nlm.nih.gov/articles/PMC8987506/
6. Costa, P., & Sousa Lobo, J. M. (2001). Modeling and comparison of dissolution profiles. *European Journal of Pharmaceutical Sciences*, *13*(2), 123–133. https://doi.org/10.1016/S0928-0987(01)00095-1
7. Derringer, G., & Suich, R. (1980). Simultaneous optimization of several response variables. *Journal of Quality Technology*, *12*(4), 214–219. https://doi.org/10.1080/00224065.1980.11980968
8. Devarajan, P. V., & Tarate, B. (2017). Lapatinib Ditosylate solid dispersions: A novel oral nanocrystalline formulation. *International Journal of Pharmaceutics*, *528*(1–2), 19–31. https://doi.org/10.1016/j.ijpharm.2017.05.067
9. European Medicines Agency. (n.d.). *Lapatinib film-coated tablet 250 mg product-specific bioequivalence guidance*.

https://www.ema.europa.eu/en/documents/scientific-guideline/lapatinib-film-coated-tablet-250-mg-product-specific-bioequivalence-guidance-first-version-1st-draft_en.pdf
10. Ferreira, S. L. C., Bruns, R. E., Ferreira, H. S., Matos, G. D., David, J. M., Brandão, G. C., da Silva, E. G. P., Portugal, L. A., dos Reis, P. S., Souza, A. S., & dos Santos, W. N. L. (2007). Box–Behnken design: An alternative for the optimization of analytical methods. *Analytica Chimica Acta*, *597*(2), 179–186. https://doi.org/10.1016/j.aca.2007.07.011
11. Gibaldi, M., & Perrier, D. (1982). *Pharmacokinetics* (2nd ed.). Marcel Dekker.
12. Higuchi, T., & Connors, K. A. (1965). Phase-solubility techniques. *Advances in Analytical Chemistry and Instrumentation*, *4*, 117–212.
13. International Council for Harmonisation. (2003). *ICH Q1A(R2): Stability testing of new drug substances and products*. https://www.ich.org/
14. Journal of Applied Pharmaceutical Science. (2024). Insights from model drug study of lapatinib. *Journal of Applied Pharmaceutical Science*. https://japsonline.com/abstract.php?article_id=4247&sts=2
15. Koch, K. M., Reddy, N. J., Cohen, R. B., Lewis, N. L., Whitehead, B., Mackay, K., Stead, A., Beelen, A. P., & Lewis, L. D. (2009). Effects of food on the relative bioavailability of lapatinib in cancer patients. *Journal of Clinical Oncology*, *27*(8), 1191–1196.
16. K. Pavan Kumar and M. Kannadasan. Therapeutic Horizons of Autophagy and Apoptosis in Colorectal Cancer: A Translational Perspective from Molecules to Medicine. International Journal of Pharmaceutical Biological and Chemical Sciences. 2025 14(1): 36-46.
17. K. Pavan Kumar and M. Kannadasan. Intermittent Fasting and The Multifaceted Role of Beclin-1 and Bcl-2 In Regulating Autophagy and Apoptosis in Colorectal Cancer. Journal of Chemical and Pharmaceutical Sciences. 2025 18 (2): 103-114.
18. Korsmeyer, R. W., Gurny, R., Doelker, E., Buri, P., & Peppas, N. A. (1983). Mechanisms of solute release from porous hydrophilic polymers. *International Journal of Pharmaceutics*, *15*(1), 25–35. https://doi.org/10.1016/0378-5173(83)90064-9
19. K. Pavan Kumar and Amit Kumar. Modulation Of Beclin-1 and Bcl-2 Expression by Intermittent Fasting In CRC: Links to Autophagy and Apoptosis. International Journal of Pharmacy and Biological Sciences. 2025 15 (4): 91-115.
20. K. Pavan Kumar and Amit Kumar. Intermittent Fasting-Induced Autophagy and Apoptosis in Colorectal Carcinoma: The Role of Beclin-1 and Bcl-2. International Journal of Pharmaceutical Biological and Chemical Sciences. 2025 14 (4): 26-38.
21. Kokkula PavanKumar, Rajeev Imadi, Prasad Garrepally, S Nikitha Anthelmintic Activity of Some Medicinal Plants: A Short Review, International Journal of Pharmacy and Biological Sciences,9(2):605 611(2019.
22. Kokkula Pavan Kumar, Ampati Srinivas and Prasad Garrepally, Hyperthermia has consistently improved the efficacy of radiotherapy and chemotherapy for many types of cancers, Journal of Stem cell Research and Therapeutics International, 1(003):1-3(2019).
23. Kokkula Pavan Kumar, Ampati Srinivas and Prasad Garrepally, Subcutaneous DL technique has proven to be an adequate host for human embryonic stem cells, Journal of Stem cell Research and Therapeutics International, 1(004):1-3(2019).
24. Kokkula Pavan Kumar, Boda Rambabu, Investigational studies on carcinoma in male SD rats, International Journal of Research and Analytical Reviews,6(2):654-662(2019).
25. K. Pavan Kumar, G. Venkateshwarlu, Navaneeth Kumar, Mukesh Sharma, Rekha Pal, Taniya Rawat, E. Rajeswari, Wound healing activity of Indian Medicinal Plants, High Technology Letters, 28(2):1 7(2022).
26. K. Pavan Kumar, G. Venkateshwarlu, Mukesh Chandra Sharma, Govind pal, Rekha pal, Taniya Rawat, Invitro anthelmintic activity of alcoholic and methanolic extracts of seeds of Panicum miliaceum in Indian adult earthworm, High Technology Letters, 28(1): 800 809(2022).
27. Martignoni, M., Groothuis, G. M. M., & de Kanter, R. (2006). Species differences between mouse, rat, dog, monkey and human CYP-mediated drug metabolism, inhibition and induction. *Expert Opinion on Drug Metabolism & Toxicology*, *2*(6), 875–894. https://doi.org/10.1358/dof.2006.031.09.1041229
28. National Cancer Institute. (2007). *Lapatinib Ditosylate*. https://www.cancer.gov/about-cancer/treatment/drugs/lapatinibDitosylate
29. Osmani, R. A. M., Aloorkar, N. H., Ingale, D. J., Kulkarni, P. K., Hani, U., Bhosale, R. R., & Jayachandra, D. (2015). Novel cyclodextrin Nanosponges for delivery of calcium in hyperphosphatemia. *International Journal of Biological Macromolecules*, *75*, 149–159.
30. Percie du Sert, N., Hurst, V., Ahluwalia, A., Alam, S., Avey, M. T., Baker, M., Browne, W. J., Clark, A., Cuthill, I. C., Dirnagl, U., Emerson, M., Garner, P., Holgate, S. T., Howells, D. W., Karp, N. A., Lazic, S. E., Lidster, K., MacCallum, C. J., Macleod, M., …

Wurbel, H. (2020). The ARRIVE guidelines 2.0: Updated guidelines for reporting animal research. *PLoS Biology*, *18*(7), e3000410. https://doi.org/10.1371/journal.pbio.3000410

31. Polli, J. W., Humphreys, J. E., Harmon, K. A., Castellino, S., O'Mara, M. J., Olson, K. L., John-Williams, L. S., Koch, K. M., & Serabjit-Singh, C. J. (2008). The role of efflux and uptake transporters in [N-{3-chloro-4-[(3-fluorobenzyl)oxy]phenyl}-6-[5-({[2-(methylsulfonyl)ethyl]amino}methyl)-2-furyl]-4-quinazolinamine (GW572016, lapatinib) disposition and drug interactions. *Drug Metabolism and Disposition*, *36*(4), 695–701. https://doi.org/10.1124/dmd.107.018374
32. Reddy, S., Kumar, T. P., & Rao, Y. M. (2022). Formulation of lipid-based nanoparticles for simultaneous delivery of lapatinib and paclitaxel. *Pharmaceuticals*, *15*(12), 1462. https://pmc.ncbi.nlm.nih.gov/articles/PMC9784347/
33. Ritger, P. L., & Peppas, N. A. (1987). A simple equation for description of solute release. II. Fickian and anomalous release from swellable devices. *Journal of Controlled Release*, *5*(1), 37–42. https://doi.org/10.1016/0168-3659(87)90035-6
34. Swaminathan, S., Cavalli, R., & Trotta, F. (2024). Development of diphenyl carbonate-crosslinked cyclodextrin Nanosponges for improved oral bioavailability. *International Journal of Nanomedicine*, *18*, 2231–2249. https://pmc.ncbi.nlm.nih.gov/articles/PMC10150753/
35. Trotta, F., Zanetti, M., & Cavalli, R. (2012). Cyclodextrin-based Nanosponges as drug carriers. *Beilstein Journal of Organic Chemistry*, *8*, 2091–2099. https://doi.org/10.3762/bjoc.8.235
36. U.S. Food and Drug Administration. (2010). *TYKERB (lapatinib) tablets: Prescribing information*. https://www.accessdata.fda.gov/drugsatfda_docs/label/2010/022059s007lbl.pdf
37. Zhang, Y., Huo, M., Zhou, J., & Xie, S. (2010). PK Solver: An add-in program for pharmacokinetic and pharmacodynamic data analysis in Microsoft Excel. *Computer Methods and Programs in Biomedicine*, *99*(3), 306–314. https://doi.org/10.1016/j.cmpb.2010.01.007